JACS
JOURNAL OF THE AMERICAN CHEMICAL SOCIETY
Article
pubs.acs.org/JACS

Guest Programmable Multistep Spin Crossover in a Porous 2-D Hofmann-Type Material

Michael J. Murphy, Katrina A. Zenere, Florence Ragon, Peter D. Southon, Cameron J. Kepert,* and Suzanne M. Neville*

School of Chemistry, The University of Sydney, Sydney, NSW 2006, Australia

Supporting Information

ABSTRACT: The spin crossover (SCO) phenomenon defines an elegant class of switchable materials that can show cooperative transitions when long-range elastic interactions are present. Such materials can show multistepped transitions, targeted both fundamentally and for expanded data storage applications, when antagonistic interactions (i.e., competing ferro- and antiferro-elastic interactions) drive concerted lattice distortions. To this end, a new SCO framework scaffold, $[Fe^{II}(bztrz)_2(Pd^{II}(CN)_4)]\cdot n(guest)$ (bztrz = (*E*)-1-phenyl-*N*-(1,2,4-triazol-4-yl)-methanimine, **1·*n*(guest)**), has been prepared that supports a variety of antagonistic solid state interactions alongside a distinct dual guest pore system. In this 2-D Hofmann-type material we find that inbuilt competition between ferro- and antiferro-elastic interactions provides a SCO behavior that is intrinsically frustrated. This frustration is harnessed by guest exchange to yield a very broad array of spin transition characters in the one framework lattice (one- (**1·(H_2O,EtOH)**), two- (**1·3H_2O**) and three-stepped (**1·~2H_2O**) transitions and SCO-deactivation (**1**)). This variety of behaviors illustrates that the degree of elastic frustration can be manipulated by molecular guests, which suggests that the structural features that contribute to multistep switching may be more subtle than previously anticipated.

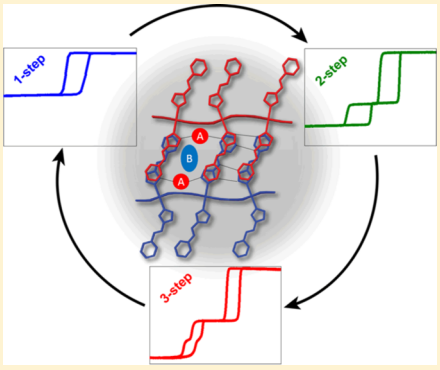

INTRODUCTION

The spin crossover (SCO) phenomenon, in which external stimuli (such as temperature, pressure, light, or magnetic field) drive an electronic conversion between two local spin states with differing magnetic, optical, electrical and structural properties, represents one of the most versatile classes of molecule-based switches.[1] Underlying the SCO effect in the solid state are strong elastic interactions between SCO sites, which commonly favor abrupt spin transitions with thermal hysteresis (i.e., memory effects).[2] Various synthetic strategies have been developed toward achieving high levels of cooperativity in these systems, for example through the use of intermolecular interactions in supramolecular systems and coordination bonds in polymeric systems.[1] However, it remains the case that the extreme sensitivity of SCO behavior to subtle lattice effects often impedes the ability to predict and regulate switching properties.[3] This sensitivity to chemical environment has been exploited both in porous framework SCO materials[4] and in various nonporous molecular materials that allow guest exchange[5] to explore the influence of guest-induced structural perturbation on SCO properties, leading in turn to a new mechanism for guest sensing. Notable among such porous materials are Hofmann-type systems, for which SCO properties such as transition temperature and thermal hysteresis may experience significant guest-induced perturbation, and which in some cases show sensitivity at room temperature.[1b,4n]

Recently, it has emerged that, beyond their porous capacity, Hofmann-type materials (and related 2-D framework materials) are suitable candidates for producing multistepped SCO behavior.[6] Materials that display stepwise transitions are sought after as they lead to high order data storage possibilities such as ternary and quaternary processing. A newly developed theoretical model shows that elastic frustration arising from antagonistic solid state interactions provides a route toward generating and stabilizing mixed high spin (HS)/low spin (LS) fractional states, leading to multistepped thermal spin transitions.[7] Hofmann-type materials appear to intrinsically support such elastic frustration due both to their ability to maintain various distorted geometries, such as layer undulations, and to experience antagonistic ligand−ligand and ligand−guest interactions in the interlayer spacing. Given that the interlayer spacing in Hofmann-type materials is readily tuned by ligand substitution this provides a versatile means to tailor such interactions.

In a new approach, we show that the porous facet of Hofmann-type materials, in combination with their intrinsic disposition toward elastic frustration, can be exploited to vary the number of SCO steps displayed by the one material. While many reports of Hofmann-type materials exist where the spin transition temperature is modulated by guest variation, guest enclathration rarely influences SCO character (i.e., the number of steps and transition completion).[8] Here, the broadest diversity of spin transition character yet reported in a single

Received: December 7, 2016
Published: January 3, 2017

DOI: 10.1021/jacs.6b12465
J. Am. Chem. Soc. 2017, 139, 1330−1335

system (encompassing one-, two- and three-stepped SCO character and SCO-deactivation) is enabled due to the presence of a dual-guest binding pocket that has distinct guest affinities and interaction modes. This being the first such account of guest programmable multistep SCO, the findings provide evidence that the multistep process may be more subtle than thus far anticipated, and open new pathways for guest-induced SCO phenomena.

RESULTS AND DISCUSSION

Framework Synthesis and Structure. The framework scaffold of $[Fe^{II}(bztrz)_2(Pd^{II}(CN)_4)]\cdot n(guest)$, **1·*n*(guest)** (bztrz = (*E*)-1-phenyl-*N*-(1,2,4-triazol-4-yl)methanimine) is readily prepared by slow diffusion of $[Fe(ClO_4)_2]\cdot n(H_2O)$, $K_2[Pd(CN)_4]$ and bztrz in ethanol and water (50:50 vol %) to produce bright yellow square plate crystals of **1·(H$_2$O,EtOH)**. Single crystal X-ray diffraction analysis of this phase (200 K; Table S1) reveals undulating Hofmann-type layers of composition $[Fe^{II}Pd(CN)_4]$ spaced by bztrz ligands bound axially to the Fe^{II} sites through N1 of the 1,2,4-triazole group (Figure 1(a)). The bztrz ligands from adjacent layers overlap in a "head-to-tail" fashion via π-stacking (Figure 1(b)), thus providing a pseudo-3-D character to the framework structure.

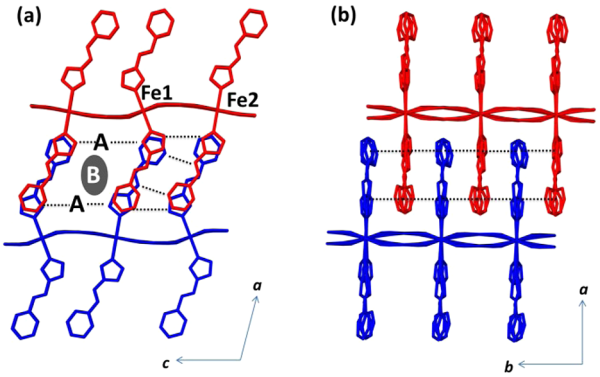

Figure 1. Two adjacent 2-D layers of 1·*n*(guest), viewed along the (a) *b*-axis and (b) *c*-axis, highlighting the distinct Fe^{II} sites (**Fe1** and **Fe2**), alternating arrays of ligand···ligand interactions, and guest-filled channels; the two binding sites in the pores (**A** and **B**) with distinct host–guest interaction modes, and π-stacking with layer interdigitation.

The Hofmann layer undulation arises due to the presence of two distinct Fe^{II} sites (**Fe1** and **Fe2**; Figure 1(a)) which vary in their tilt away from an idealized planar layer (Table S3). At this temperature both Fe^{II} sites are in the HS state and **Fe1** adopts a slightly more regular octahedral geometry (Table S3).

The most important feature of this layer undulation is that it creates two distinct ligand spacings: (1) pairs of closely related ligands interact in a series of hydrogen-bonding interactions, and (2) larger ligand spacings house guest molecules (Figure 1(a)). There are two distinct guest docking sites within these pores with differing guest affinities and guest interaction modes (Figure 1(a); **A** and **B**). At the "**A** site", water molecules interact at close distance with the free nitrogen atom on the 1,2,4-triazole rings through hydrogen bonding interactions (Figure S2). Loosely bound ethanol molecules occupy the "**B** site", being held in place only by van der Waals interactions.

This versatile dual-binding pore system is an important structural design feature of this framework scaffold, which has allowed a range of guest substituted and partially desolvated phases to be produced: **1·(H$_2$O,EtOH)**; **1·3H$_2$O**; **1·~2H$_2$O**; and **1**. Water adsorption measurements highlight the distinction between these guest sites, showing stepped uptake at distinct partial pressures (Figure 2). The strongly hydrophilic nature of

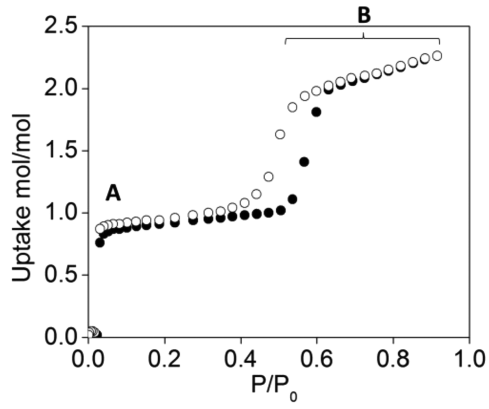

Figure 2. Water vapor adsorption (closed circles) and desorption (open circles) isotherms for **1** at 25 °C. Guest docking site regions **A** and **B** indicated.

the **A** site is indicated by the abrupt uptake of one water molecule at very low partial pressures (~0.03 P/P_0). It is not until beyond 0.5 P/P_0 that the **B** site is accessed (indicating a less favorable adsorption without direct host contacts), producing the partially and fully hydrated phases **1·~2H$_2$O** and **1·3H$_2$O** at or above 0.6 P/P_0, respectively. Owing to the necessity to include a mixed solvent media in the framework scaffold synthesis so as to prevent the precipitation of side-products such as metal oxides, the hydrated phases were produced by guest exchange from **1·(H$_2$O,EtOH)**. The guest exchange process from **1·(H$_2$O,EtOH)** to **1·3H$_2$O** is achieved simply by exposure of the crystalline material to atmospheric conditions or by immersion in water. With thermogravimetry (and subsequent crystallography) indicating a total of three water molecules per Fe^{II} site and isothermal gravimetry slightly less than three, we have assigned this phase as a trihydrate (**1·3H$_2$O**; Figure S11). The partially hydrated species **1·~2H$_2$O** is produced by heating **1·3H$_2$O** to 50 °C, as determined by thermogravimetry (Figure S11). The empty framework lattice is produced via heating any of the solvated phases above 90 °C. Despite the water adsorption measurements revealing a clear step at **1·H$_2$O** we were unable to access this phase either structurally or magnetically.

Fortuitously, the guest exchange process from **1·(H$_2$O,EtOH)** to **1·3H$_2$O** proceeds via a single-crystal to single-crystal transformation with no apparent loss in crystal integrity, allowing detailed structural analyses to be performed; attempts at similar analyses of **1·~2H$_2$O** and **1** were hampered by loss of monocrystallinity.

Structural analysis of **1·3H$_2$O** at 200 K reveals a phase isostructural to **1·(H$_2$O,EtOH)** with little variation to unit cell parameters or volume (Table S2). The overall structural topology is unchanged and, within the pore cavity, the 1,2,4-triazole to water hydrogen bonding interactions are retained as per **1·(H$_2$O,EtOH)**. Within the central pore cavity (site **B**) the ethanol molecules of the parent phase have been replaced by two water molecules, one of which is disordered over two positions (Figure S6). At this temperature the Fe–N bond lengths indicate that both Fe^{II} sites are in the HS state (Table

DOI: 10.1021/jacs.6b12465
J. Am. Chem. Soc. 2017, 139, 1330–1335

S3). Most notably, at this temperature both Fe^{II} sites display a similar degree of octahedral distortion, in contrast to that seen in **1·(H$_2$O,EtOH)**, in which **Fe1** is more regular than **Fe2**.

Guest Dependent Spin Crossover Properties. Temperature dependent magnetic susceptibility measurements revealed remarkably distinct SCO behaviors for each of the phases, encompassing one-, two- and three-stepped SCO transitions and SCO-deactivation (Figure 3). For **1·(H$_2$O,EtOH)**, an

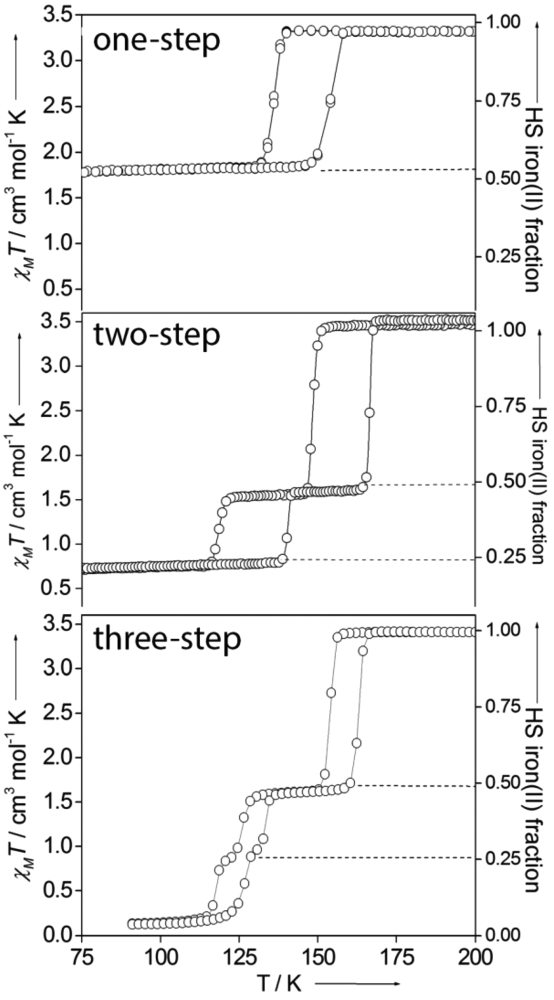

Figure 3. Variable temperature magnetic susceptibility data of **1·(H$_2$O,EtOH)** (top), **1·3H$_2$O** (middle), **1·∼2H$_2$O** (bottom). Scan rate of 2 K min^{-1} in sweep mode. HS Fe^{II} fraction for each step indicated (---).

abrupt single-step spin transition with thermal hysteresis results ($T_{1/2}\downarrow\uparrow$ = 135 K, 154 K; ΔT = 19 K; Figure 3(a)). The $\chi_M T$ values below 140 K indicate a 50% conversion of HS Fe^{II} sites to the LS state.

Exchange of guest ethanol with water in the framework **B** site to yield **1·3H$_2$O** leads to a two-step spin transition characterized by two closed hysteresis loops (Figure 3(b)). The high temperature hysteresis loop corresponds to a 50% conversion of HS Fe^{II} sites to the LS state, as per **1·(H$_2$O,EtOH)**, but increased in temperature ($T_{1/2}\downarrow\uparrow$ = 148, 166 K; ΔT = 18 K). The $\chi_M T$ values of the lower temperature hysteresis loop indicate that 25% of the Fe^{II} sites remain in the HS state ($T_{1/2}\downarrow\uparrow$ = 118, 140 K, ΔT = 22 K). Both loops display a similar degree of thermal abruptness as the single loop of the parent phase, with the temperature range of each step being substantially less than the shifts in $T_{1/2}\downarrow\uparrow$ observed. This, and the integral HS:LS ratios observed, suggests a very high degree of sample homogeneity. Further, it indicates that guest exchange does not in any way compromise the cooperative nature of the framework.

Subsequent partial desorption of guest water from **1·3H$_2$O** to yield **1·∼2H$_2$O** leads to a three-step SCO transition characterized by two open hysteresis loops (Figure 3(c)). To our knowledge this is the first three-step SCO of its type. A three-step SCO was reported in a Hofmann-type material which shows a single hysteresis loop,[6a] but the majority of other such transitions (of which there are few) show only subtle hysteresis and ill-defined steps.[6e,8a,9] The overlapping thermal hysteresis of the multistep transitions in this example results in formal tristability at fixed temperatures, which is rare. Detailing the magnetic behavior of **1·∼2H$_2$O**, the high temperature hysteresis loop is approximately at the same temperature, but with a smaller width, as that of **1·3H$_2$O** ($T_{1/2}\downarrow\uparrow$ = 153, 163 K; ΔT = 10 K). This step again corresponds to a conversion of half of the Fe^{II} sites from HS to LS. The lower temperature hysteresis loop proceeds in two steps, where the steps occur at 0.5, 0.25, and 0.0 HS Fe^{II} fractions. Overall, the hysteresis loop size and width is commensurate with that of **1·3H$_2$O** ($T_{1/2}\downarrow\uparrow$ = 116, 134 K; ΔT = 18 K). Again, the retention of abrupt steps and integral HS:LS ratios across the full temperature range implies an equivalent level of hydration across the crystallite sample, demonstrating also that despite the loss of mono-crystallinity the sample retains its intrinsically high degree of cooperativity.

With further guest removal to generate **1**, a HS character is obtained over all temperatures (Figure S16).

Magnetostructural Rationalization. In delineating the unprecedented breadth of SCO character variation attained within this framework scaffold, which occurs with seemingly minor guest modification, we now look in detail at the variation in structure over the spin transition process for **1·(H$_2$O,EtOH)** and **1·3H$_2$O** (Figure 4). First, to confirm bulk phase purity and magneto-structural behavior, variable temperature synchrotron powder X-ray diffraction measurements were conducted over the SCO temperature range (200−100−200 K). For both phases, the peak evolution and lattice cell parameters mimic those of the magnetic measurements, including the one- and two-step SCO characters respectively (Figure 5 and Figure S17−S18). As noted above, single crystal diffraction data collected at 200 K on these phases reveal HS Fe^{II} sites for both **Fe1** and **Fe2** (Figure 4(a)). Upon cooling to the next plateau (100 K for **1·(H$_2$O,EtOH)** and 130 K for **1·3H$_2$O**), structural analyses reveal that the **Fe1** sites remain HS and the **Fe2** sites transition to the LS state; these varying sites are distributed in distinct alternating stripes within each layer (Figure 4(b); Table S1−S3; Figures S3 and S7). In both phases, it is notable that while the octahedral distortion decrease for **Fe2** as it undergoes spin transition (Σ_{Fe2} = 11.1 to 3.8° and 11.0 to 3.5° for **1·(H$_2$O,EtOH)** and **1·3H$_2$O** respectively), it increases significantly for **Fe1** (Σ_{Fe1} = 9.4 to 14.4° and 11.4 to 16.4° for **1·(H$_2$O,EtOH)** and **1·3H$_2$O** respectively). This increased distortion likely acts to stabilize the HS state at this **Fe1** site, representative of antiferroelastic lattice coupling. A similar antagonistic cooperative effect has been noted in related 2-D Hofmann-type materials[6c,f] and other nonrelated materials.[10]

Notably, conversion from **1·(H$_2$O,EtOH)** to **1·3H$_2$O** leads to an increase in the octahedral distortion of **Fe1**, an effect that is apparent both in the HS and 1:1 HS:LS states. At first glance,

DOI: 10.1021/jacs.6b12465
J. Am. Chem. Soc. 2017, 139, 1330−1335

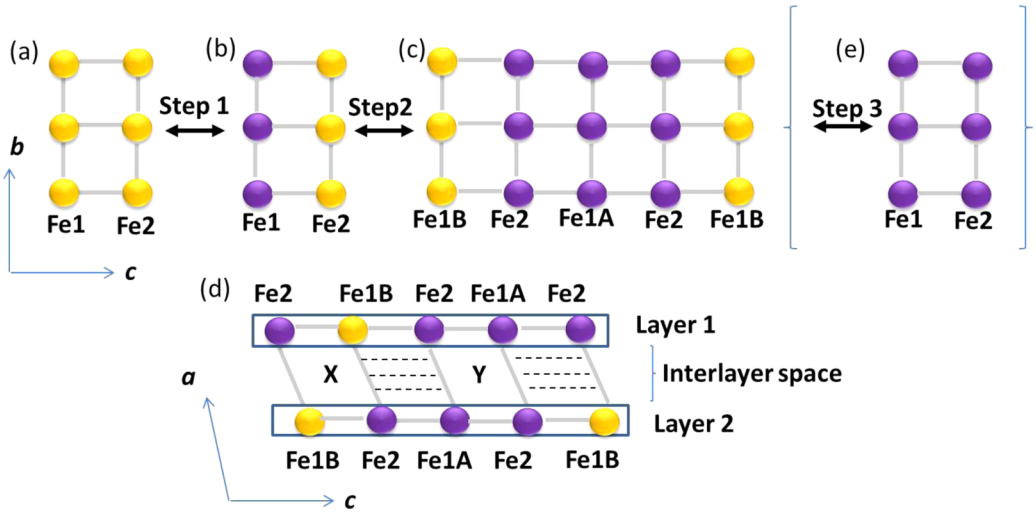

Figure 4. Schematic of the spin state transition of Fe^{II} sites within a single Hofmann layer in **1·3H$_2$O** for the two-step transition at (a) 1.0 HS fraction, (b) 0.5 HS fraction, (c) 0.25 HS fraction. (d) Two layer schematic showing the type **X** and **Y** pores surrounded by differing numbers of HS and LS sites. (a–c) is also the likely structural pathway for **1·∼2H$_2$O** including (e) the 0.0 HS fraction state.

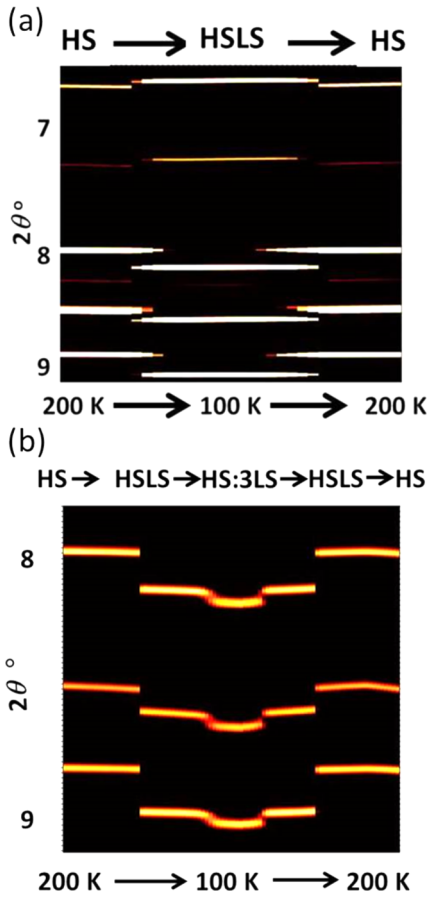

Figure 5. Variable temperature powder X-ray diffraction of (a) **1·(H$_2$O,EtOH)** and (b) **1·3H$_2$O** (200–100–200 K) showing the stepwise shift of Bragg peaks mimicking the one- and two-step SCO transition of the magnetic data, respectively.

it is therefore somewhat counterintuitive that it is the latter phase that undergoes further SCO upon continued cooling. In probing the structural evolution associated with this, we note first that, in contrast to the symmetry equivalence of the 1.0 to 0.5 HS fractional steps of both phases, conversion to the 0.25 HS fractional of **1·3H$_2$O** occurs via a crystallographic phase transition from *C*-centered to primitive monoclinic symmetry (*C*2/*c* to *P*2$_1$/*n*, Figure S4, Table S2). This symmetry reduction results in a conversion from two to three crystallographically distinct Fe^{II} sites, with **Fe1** splitting into two inequivalent sites (**Fe1A** and **Fe1B**; Figure 4(c)). Average Fe–N bond length analysis indicates that one of these sites (**Fe1B**) remains HS and the other (**Fe1A**) converts to LS (Table S3). Thus, overall a 1HS:3LS ratio of Fe^{II} sites is generated, consistent with the 0.25 HS Fe^{II} fraction observed magnetically (this distribution arising from a 1**Fe1A**^{LS}:1**Fe1B**^{HS}:2**Fe2**^{LS} ratio). As per the 0.5 fraction plateau stabilization, we find that an increase in regularity at the crossover site (Σ_{Fe1B} = 16.4 to 5.2°) comes at the expense of increased distortion at the remaining HS site (Σ_{Fe1A} = 16.4 to 18.4°), thus acting to disfavor its conversion to the LS state.

There are two possible pathways for the mixed HS:LS state to convert simply to the 1HS:3LS state within each Hofmann layer. First, the HS 1-D stripes could transition to an alternating chain of -HS-LS-HS-LS- sites (such that each HS site is surrounded by LS nearest neighbors) and, second, alternate entire HS stripes could convert to the LS state (i.e., distinct -HS-HS-HS-HS- and -LS-LS-LS-LS- stripes, such that each HS site is surrounded by two LS and two HS nearest neighbors). Structural analysis shows that it is the latter arrangement that occurs, such that the repeat motif of each Hofmann layer is three consecutive LS stripes followed by one HS stripe, as depicted in Figure 4(c). A 3-D rather than just 2-D crystallographic ordering of this arrangement occurs, with the registry of neighboring layers (Figure 4(d)) being facilitated by the ligand–ligand and potentially also host–guest interactions.

In probing the role of the guest water molecules in this novel conversion, we note first that two distinct pore environments, **X** and **Y** (Figure 4(d)), are generated through the phase transition to the 0.25 HS lattice state. Distinguishing these, pore **X** is bounded by two HS and two LS Fe^{II} sites and pore **Y** by four LS Fe^{II} sites. As a consequence of the difference in Fe–N bond lengths of LS compared to HS Fe^{II} sites, the volume of pore **Y** is markedly smaller than that of pore **X** (**X**: 222 Å^3; **Y**: 195 Å^3).[11] Concomitant with this distinction is a clear difference in guest molecule location; pore **X** contains two ordered and one

DOI: 10.1021/jacs.6b12465
J. Am. Chem. Soc. 2017, 139, 1330–1335

disordered water molecule, whereas pore **Y** contains three ordered water molecules (Figure S7). The absence of the 0.5 to 0.25 HS step in **1·(H$_2$O,EtOH)** suggests that ethanol loading within site **B** of the pores yields insufficient structural flexibility (which may include guest mobility) for the 0.25 HS lattice state to be stabilized. While low temperature transitions can be subject to kinetic freezing effects, the exact fractional trapping at this 0.25 HS step supports our belief that this is a thermodynamic rather than kinetic phase.[12] Given the complex nature of the host−guest interactions and their contribution to the overall lattice energetics, it is unclear the extent to which the guest order/disorder in **1·3H$_2$O** is a consequence of, rather than a contributor toward, the stabilization of the 0.25 HS lattice state. What is clear, however, given the observed perturbation in properties, is that elastic interactions between the host lattice and these site **B** guests, while comparatively weak, play an important role in modifying the crossover behavior. In the simplest terms we can rationalize the spin state ordering as being favored in part due to internal pressure effects associated with the progressive decrease in kinetic volume of the adsorbed water molecules upon cooling, but note that such a rationalization does not adequately consider the complex nature of these interactions.

Further insight into the role of included guests on the lattice energetics comes when we look to the partially hydrated phase **1·∼2H$_2$O**. Here, a complete SCO is evidenced such that a final 0.25 to 0.0 HS fraction step is now present. In the absence of structural data on this phase, variable scan rate studies (0.5, 1, 2, and 4 K min^{-1}), which were conducted as standard practice on all phases, provide some useful insight into the lattice changes involved. In comparing across **1·(H$_2$O,EtOH)**, **1·3H$_2$O** and **1·∼2H$_2$O** we found that the thermal hysteresis loops for the 1.0 to 0.5 HS conversion are widened with increasing scan rate (Figures S13−S15), as is broadly consistent with standard temperature lag and transition enthalpy considerations.[10,13] However, it is notable that the low temperature hysteresis loops of both **1·3H$_2$O** and **1·∼2H$_2$O** (the latter incorporating a double step) show significant scan rate dependence in the cooling sweep, which is notably more pronounced than that of the other loops, and almost no variance on the warming sweep; similar behavior has been seen in other systems and attributed to structural phenomena occurring on a longer time scale than the experimental scan rate.[14] Here, the observation of a pronounced scan rate broadening of the 0.5 to 0.25 HS conversion of **1·3H$_2$O** (Figure S14) is consistent with there being a relatively slow ordering of guest water molecules at site **B** within half of the pores, as described above. The observation of a comparable scan rate dependence in **1·∼2H$_2$O** (Figure S15) suggests that a similar effect is present, although now involving the ordering of a single rather than two water guests within site **B** of the pores. The fact that this rate dependency is observed over the entire 0.5 to 0.25 to 0.0 HS conversion suggests that water molecule reorganization occurs over both steps, rather than just the 0.5 to 0.25 portion, with stepwise ordering in pores **Y** then **X** corresponding to each partial crossover step such that the thermodynamic stabilization of the 0.25 HS lattice state again occurs concomitantly with a mixture of ordered and disordered guest water molecules.

CONCLUSIONS

In summary, we present a new spin crossover framework material in which a diverse network of host−host and host−guest interactions gives rise to a competition between antagonistic ferro- and antiferro-elastic interactions that drive SCO related lattice distortions. While this general synthetic strategy has been successful in the past in generating multistepped spin transitions spanning two- to four-stepped characters,[6c,f,g] an important distinction here is that a unique pore environment is present which has allowed the fine-tuning of guest contents to yield a range of host−guest interaction modes. Through exploiting the relatively labile nature of the internal pore space, three distinct guest-loaded phases have been accessed. Despite the modification of pore contents being seemingly minor, remarkably distinct SCO behaviors are produced, spanning one-, two- and three-stepped behaviors. Collectively, this demonstrates that the manipulation of host−guest chemistry provides significantly enhanced scope for accessing a broad diversity of SCO properties in the one material.

Beyond the novelty of the observed behaviors, the rationalization of these with respect to the precise internal pore loading provides important insight into the structural features that favor multistepped spin switching. A recently developed theoretical model and recently reported multistep SCO materials[6b−d,7] show that elastic frustration generated through antagonistic solid state interactions assist in stabilizing fractional high and low spin phases. In the Hofmann-type system presented here, the ligand···ligand and ligand···guest interactions provide a significant breadth of competitive interactions, with it being evident that guest-mediated elastic interactions play an important role in influencing the stabilization of mixed spin states. This in turn suggests that the structural features that influence the energetic competition between antagonistic interactions are more subtle than may have been previously envisaged.

When viewed in combination, these observations highlight the predilection of Hofmann-type SCO materials to accommodate varying types of structural distortion, with each of the 2-D spin state striped arrangements seen here appearing to be stabilized by geometric competition between Fe^{II} crossover sites within the Hofmann layer and their combined influence on its degree of distortion; indeed, it is this aspect that appears to make Hofmann-type materials particularly suitable for multistep SCO transitions. Most specifically in this example, the incorporation of an asymmetric ligand acts to enhance the favorability of intermediate lattice spin states, with guest variation within a dual pore system then uniquely giving access to multiple behaviors through perturbation of both the host−host and host−guest interactions, which compete collectively in an antagonistic manner. This competition between ferro- and antiferro-elastic interactions results in lattice frustration uniquely affording temperature- and guest-dependent access to an array of different 3-D spin state configurations.

With a view to future goals of incorporating spin switching materials into device technologies, we note that the variation of included guest molecules represents a particularly convenient means for manipulating desired spin switching behaviors within a material, including with the achievement of multistability as presented here. Moreover, exploitation of the dynamic nature of these guests, as manifested both by their reversible exchange and by their variable orientation and location within the pores, points to more elaborate mechanisms for guest-sensing than previously achieved, in which guest species may be identified through fractional changes in the extent of lattice spin switching.

DOI: 10.1021/jacs.6b12465
J. Am. Chem. Soc. 2017, 139, 1330−1335

■ ASSOCIATED CONTENT

Supporting Information

The Supporting Information is available free of charge on the ACS Publications website at DOI: 10.1021/jacs.6b12465.

Experimental information and synthesis and characterization of materials (PDF)
Crystal data, CCDC 1038384 (CIF)
Crystal data, CCDC 1038385 (CIF)
Crystal data, CCDC 1038386 (CIF)
Crystal data, CCDC 1038387 (CIF)
Crystal data, CCDC 1038388 (CIF)

■ AUTHOR INFORMATION

Corresponding Authors

*cameron.kepert@sydney.edu.au
*suzanne.neville@sydney.edu.au

ORCID

Suzanne M. Neville: 0000-0003-4237-4046

Notes

The authors declare no competing financial interest.

■ ACKNOWLEDGMENTS

This work was supported by Fellowship and Discovery Project funding from the Australian Research Council. Use of the Advanced Photon Source was supported by the U.S. Department of Energy, Office of Science, Office of Basic Energy Sciences, under Contract No. DE-AC02-06CH11357. Travel to the APS was funded by the International Synchrotron Access Program (ISAP) managed by the Australian Synchrotron and funded by the Australian Government. We thank Dr G. J. Halder for beamline support.

■ REFERENCES

(1) (a) Gütlich, P.; Goodwin, H. A. *Top. Curr. Chem.* **2004**, *233*, 1. (b) Gütlich, P.; Gaspar, A. B.; Garcia, Y. *Beilstein J. Org. Chem.* **2013**, *9*, 342. (c) Halcrow, M. A. *Spin-Crossover Materials: Properties and Applications*; John Wiley & Sons, 2013.

(2) Spiering, H.; Willenbacher, N. *J. Phys.: Condens. Matter* **1989**, *1*, 10089.

(3) Halcrow, M. A. *Chem. Soc. Rev.* **2011**, *40*, 4119.

(4) (a) Real, J. A.; Andres, E.; Muñoz, M. C.; Julve, M.; Granier, T.; Bousseksou, A.; Varret, F. *Science* **1995**, *268*, 265. (b) Halder, G. J.; Kepert, C. J.; Moubaraki, B.; Murray, K. S.; Cashion, J. D. *Science* **2002**, *298*, 1762. (c) Real, J. A.; Gaspar, A. B.; Muñoz, M. C. *Dalton Trans.* **2005**, 2062. (d) Neville, S. M.; Moubaraki, B.; Murray, K. S.; Kepert, C. J. *Angew. Chem., Int. Ed.* **2007**, *46*, 2059. (e) Halder, G. J.; Chapman, K. W.; Neville, S. M.; Moubaraki, B.; Murray, K. S.; Létard, J.-F.; Kepert, C. J. *J. Am. Chem. Soc.* **2008**, *130*, 17552. (f) Neville, S. M.; Halder, G. J.; Chapman, K. W.; Duriska, M. B.; Southon, P. D.; Cashion, J. D.; Létard, J.-F.; Moubaraki, B.; Murray, K. S.; Kepert, C. J. *J. Am. Chem. Soc.* **2008**, *130*, 2869. (g) Neville, S. M.; Halder, G. J.; Chapman, K. W.; Duriska, M. B.; Moubaraki, B.; Murray, K. S.; Kepert, C. J. *J. Am. Chem. Soc.* **2009**, *131*, 12106. (h) Ohba, M.; Yoneda, K.; Agusti, G.; Muñoz, M. C.; Gaspar, A. B.; Real, J. A.; Yamasaki, M.; Ando, H.; Nakao, Y.; Sakaki, S.; Kitagawa, S. *Angew. Chem., Int. Ed.* **2009**, *48*, 4767. (i) Southon, P. D.; Liu, L.; Fellows, E. A.; Price, D. J.; Halder, G. J.; Chapman, K. W.; Moubaraki, B.; Murray, K. S.; Létard, J.-F.; Kepert, C. J. *J. Am. Chem. Soc.* **2009**, *131*, 10998. (j) Muñoz, M. C.; Real, J. A. *Coord. Chem. Rev.* **2011**, *255*, 2068. (k) Ohtani, R.; Yoneda, K.; Furukawa, S.; Horike, N.; Kitagawa, S.; Gaspar, A. B.; Muñoz, M. C.; Real, J. A.; Ohba, M. *J. Am. Chem. Soc.* **2011**, *133*, 8600. (l) Muñoz-Lara, F. J.; Gaspar, A. B.; Aravena, D.; Ruiz, E.; Muñoz, M. C.; Ohba, M.; Ohtani, R.; Kitagawa, S.; Real, J. A. *Chem. Commun.* **2012**, *48*, 4686. (m) Aravena, D.; Castillo, Z. A.; Muñoz, M. C.; Gaspar, A. B.; Yoneda, K.; Ohtani, R.; Mishima, A.; Kitagawa, S.; Ohba, M.; Real, J. A.; Ruiz, E. *Chem. - Eur. J.* **2014**, *20*, 12864. (n) Ohtani, R.; Hayami, S. *Chem. - Eur. J.* **2017**, DOI: 10.1002/chem.201601880. (o) Romero-Morcillo, T.; Pinta, N. D. l.; Callejo, L. M.; Piñeiro-López, L.; Muñoz, M. C.; Madariaga, G.; Ferrer, S.; Breczewski, T.; Cortés, R.; Real, J. A. *Chem. - Eur. J.* **2016**, *21*, 12112. (p) Bao, X.; Shepherd, H. J.; Salmon, L.; Molnár, G.; Tong, M.-L.; Bousseksou, A. *Angew. Chem., Int. Ed.* **2013**, *52*, 1198.

(5) (a) Hostettler, M.; Törnroos, K. W.; Chernyshov, D.; Vangdal, B.; Bürgi, H.-B. *Angew. Chem., Int. Ed.* **2004**, *33*, 4589. (b) Amoore, J. J. M.; Neville, S. M.; Moubaraki, B.; Iremonger, S. S.; Murray, K. S.; Létard, J. F.; Kepert, C. J. *Chem. - Eur. J.* **2010**, *16*, 1973. (c) Li, B.; Wei, R.-J.; Tao, J.; Huang, R.-B.; Zheng, L.-S.; Zheng, Z. *J. Am. Chem. Soc.* **2010**, *132*, 1558. (d) Wei, R.-J.; Tao, J.; Huang, R.-B.; Zheng, L.-S. *Inorg. Chem.* **2011**, *50*, 8553. (e) Wang, Y.-T.; Li, S.-T.; Wu, S.-Q.; Cui, A.-L.; Shen, D.-Z.; Kou, H.-Z. *J. Am. Chem. Soc.* **2013**, *135*, 5942. (f) Costa, J. S.; Rodríguez-Jiménez, S.; Craig, G. A.; Barth, B.; Beavers, C. M.; Teat, S. J.; Aromí, G. *J. Am. Chem. Soc.* **2014**, *136*, 3869. (g) Huang, W.; Shen, F.; Zhang, M.; Wu, D.; Pan, F.; Sato, O. *Dalton Trans.* **2016**, *45*, 14911.

(6) (a) Sciortino, N. F.; Scherl-Gruenwald, K. R.; Chastanet, G.; Halder, G. J.; Chapman, K. W.; Létard, J.-F.; Kepert, C. J. *Angew. Chem., Int. Ed.* **2012**, *51*, 10154. (b) Clements, J. E.; Price, J. R.; Neville, S. M.; Kepert, C. J. *Angew. Chem., Int. Ed.* **2016**, *55*, 15105. (c) Sciortino, N. F.; Zenere, K. A.; Corrigan, M. E.; Halder, G. J.; Chastanet, G.; Létard, J.-F.; Kepert, C. J.; Neville, S. M. *Chem. Sci.* **2017**, *8*, 701. (d) Trzop, E.; Zhang, D.; Piñeiro-Lopez, L.; Valverde-Muñoz, F. J.; Muñoz, M. C.; Palatinus, L.; Guerin, L.; Cailleau, H.; Real, J. A.; Collet, E. *Angew. Chem., Int. Ed.* **2016**, *55*, 8675. (e) Ohtani, R.; Masashi, A.; Hori, A.; Takata, M.; Kitao, S.; Seto, M.; Kitagawa, S.; Ohba, M. *J. Inorg. Organomet. Polym. Mater.* **2013**, *23*, 104. (f) Klein, Y. M.; Sciortino, N. F.; Ragon, F.; Housecroft, C. E.; Kepert, C. J.; Neville, S. M. *Chem. Commun.* **2014**, *50*, 3838. (g) Milin, E.; Patinec, V.; Triki, S.; Bendeif, E.-E.; Pillet, S.; Marchivie, M.; Chastanet, G.; Boukheddaden, K. *Inorg. Chem.* **2016**, *55*, 11652. (h) Sciortino, N. F.; Ragon, F.; Zenere, K. A.; Southon, P. D.; Halder, G. J.; Chapman, K. W.; Piñeiro-López, L.; Real, J. A.; Kepert, C. J.; Neville, S. M. *Inorg. Chem.* **2016**, *55*, 10490.

(7) Paez-Espejo, M.; Sy, M.; Boukheddaden, K. *J. Am. Chem. Soc.* **2016**, *138*, 3202.

(8) (a) Yoshida, K.; Akahoshi, D.; Kawasaki, T.; Saito, T.; Kitazawa, T. *Polyhedron* **2013**, *66*, 252. (b) Bao, X.; Shepherd, H. J.; Salmon, L.; Molnár, G.; Tong, M.-L.; Bousseksou, A. *Angew. Chem., Int. Ed.* **2013**, *52*, 1198. (c) Li, J.-Y.; He, C.-T.; Chen, Y.-C.; Zhang, Z.-M.; Liu, W.; Ni, Z.-P.; Tong, M.-L. *J. Mater. Chem. C* **2015**, *3*, 7830.

(9) (a) Kosone, T.; Tomori, I.; Kanadani, C.; Saito, T.; Mochida, T.; Kitazawa, T. *Dalton Trans.* **2010**, *39*, 1719. (b) Nihei, M.; Tahira, H.; Takahashi, N.; Otake, Y.; Yamamura, Y.; Sato, K.; Oshio, H. *J. Am. Chem. Soc.* **2010**, *132*, 3553.

(10) Kulmaczewski, R.; Olguin, J.; Kitchen, J. A.; Feltham, H. L.; Jameson, G. N. L.; Tallon, J. L.; Brooker, S. *J. Am. Chem. Soc.* **2014**, *136*, 878.

(11) Spek, A. L. *Acta Crystallogr., Sect. D: Biol. Crystallogr.* **2009**, *D65*, 148.

(12) (a) Paradis, N.; Chastanet, G.; Létard, J.-F. *Eur. J. Inorg. Chem.* **2012**, *2012*, 3618. (b) Varret, F.; Boukheddaden, K.; Chastanet, G.; Paradis, N.; Létard, J.-F. *Eur. J. Inorg. Chem.* **2013**, *2013*, 763.

(13) Brooker, S. *Chem. Soc. Rev.* **2015**, *44*, 2789.

(14) (a) Seredyuk, M.; Muñoz, M. C.; Castro, M.; Romero-Morcillo, T.; Gaspar, A. B.; Real, J. A. *Chem. - Eur. J.* **2013**, *19*, 6591. (b) Miller, R. G.; Narayanaswamy, S.; Tallon, J. L.; Brooker, S. *New J. Chem.* **2014**, *38*, 1932.

DOI: 10.1021/jacs.6b12465
J. Am. Chem. Soc. 2017, 139, 1330−1335